

Efficient Nanoscale Exciton Transport in Non-Fullerene Organic Solar Cells Enables Reduced Bimolecular Recombination of Free Charges

Drew B. Riley,* Oskar J. Sandberg,* Nasim Zarrabi, Yong Ryun Kim, Paul Meredith,* and Ardan Armin*

The highest-efficiency organic photovoltaic (OPV)-based solar cells, made from blends of electron-donating and electron-accepting organic semiconductors, are often characterized by strongly reduced (non-Langevin) bimolecular recombination. Although the origins of the reduced recombination are debated, mechanisms related to the charge-transfer (CT) state and free-carrier encounter dynamics controlled by the size of donor and acceptor domains are proposed as underlying factors. Here, a novel photoluminescence-based probe is reported to accurately quantify the donor–acceptor domain size in OPV blends. Specifically, the domain size is measured in high-efficiency non-fullerene acceptor (NFA) systems and a comparative conventional fullerene system. It is found that the NFA-based blends form larger domains but that the expected reductions in bimolecular recombination attributed to the enhanced domain sizes are too small to account for the observed reduction factors. Further, it is shown that the reduction of bimolecular recombination is correlated to enhanced exciton dynamics within the NFA domains. This indicates that the processes responsible for efficient exciton transport also enable strongly non-Langevin recombination in high-efficiency NFA-based solar cells with low-energy offsets.

19%.^[1–4] A PCE of 20% is in sight, and an optimistic value of 25% is predicted.^[5] To achieve this, all loss mechanisms, however small, must be identified and overcome. These BHJs are made of blends of excitonic electron-donating (donor) and electron-accepting (acceptor) organic semiconductors that form percolated and phase-separated domains. These domains, consisting of donor- or acceptor-rich regions, act as charge collection channels to the electrodes, while the interfaces between donor and acceptor domains, consisting of small intermixed regions of donor and acceptor molecules, act as charge generation and recombination centers.^[6,7]

To maximize charge generation, the domain sizes need to be small enough to ensure that the majority of photogenerated excitons can diffuse to a donor–acceptor interface. At the interface, the exciton dissociates into a charge-transfer (CT) state by transferring an electron (hole) to the acceptor (donor) phase.^[6] Alternatively, Förster resonance energy transfer (FRET) can occur from donor (typically having larger


exciton energies than the acceptor in state-of-the-art NFA-based OPVs) to acceptor,^[8,9] followed by migration of acceptor excitons to the interface and dissociation into CT states. Once CT states are formed, owing to lower binding energy, they typically dissociate into separated free charge carriers with relatively high quantum efficiency.^[10,11]

To maximize the collection of separated charge carriers, in turn, the acceptor (donor) domains need to be large and pure enough to support efficient charge transport of electrons (holes) and minimize bimolecular recombination between separated charges. Bimolecular recombination in BHJs is commonly understood as a two-step process involving electron and hole encounter to form bound CT states and a subsequent decay of the bound states, which otherwise re-dissociate back to free charges. The bimolecular recombination rate constant (β) in many BHI devices has been observed to be orders of magnitude lower than the Langevin rate constant (β_L) expected for diffusion-limited charge-carrier recombination processes.^[10,12,13] This reduction factor ($\zeta_L = \beta_L/\beta \geq 1$) is typically attributed to a reduction (ζ_{enc}) associated with impediments to electron–hole encounters due to

1. Introduction

Recently, the power conversion efficiencies (PCEs) of bulk heterojunction (BHJ) organic photovoltaic (OPV)-based solar cells have consistently exceeded 15% with the introduction of non-fullerene acceptor (NFA) molecules and now are approaching

D. B. Riley, O. J. Sandberg, N. Zarrabi, Y. R. Kim, P. Meredith, A. Armin
Sustainable Advanced Materials (Sêr-SAM)
Department of Physics
Swansea University
Singleton Park, Swansea, Wales SA2 8PP, UK
E-mail: d.b.riley@swansea.ac.uk; o.j.sandberg@swansea.ac.uk; paul.meredith@swansea.ac.uk; ardan.armin@swansea.ac.uk

 The ORCID identification number(s) for the author(s) of this article can be found under <https://doi.org/10.1002/adma.202211174>

© 2023 The Authors. Advanced Materials published by Wiley-VCH GmbH. This is an open access article under the terms of the Creative Commons Attribution License, which permits use, distribution and reproduction in any medium, provided the original work is properly cited.

DOI: 10.1002/adma.202211174

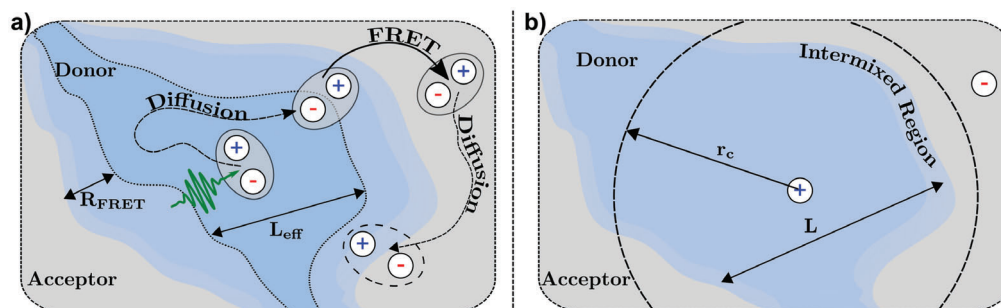


Figure 1. Charge generation and recombination processes in organic semiconductor bulk heterojunctions. a,b) Graphical representation of the domain size of a bulk heterojunction from the frame of reference of a photoexcited exciton (a) and a pair of separated charge carriers (b). r_c indicates the Coulomb capture radius.

their geometrical confinement in the respective domains,^[12,14] and a reduction (ζ_{CT}) due to the re-dissociation of CT states into free charges, such that $\zeta_L = \zeta_{enc} \zeta_{CT}$, where $\zeta_{enc} \geq 1$ and $\zeta_{CT} \geq 1$.^[15] In recently reported NFA-based organic solar cells based on low-offset donor–acceptor systems, the CT state kinetics, and thus ζ_{CT} , is further expected to be strongly influenced by excitons. Explicitly, it is expected that ζ_{CT} is inversely proportional to the exciton lifetime.^[4,16,17] However, thus far the interrelation between exciton dynamics and bimolecular recombination of free charges in NFA-based BHJs has remained unclear.

To gain further insights into exciton dynamics and bimolecular recombination of free charges in BHJs, methods to probe the morphology are needed. Studies of the surface morphology of many NFA-based BHJs via atomic force microscopy have revealed that the surface domains exhibit superior phase separation and larger domain sizes than fullerene blends.^[1,18] Further, studies using transmission electron microscopy (TEM) have indicated that this trend extends into the bulk of NFA-based BHJs.^[19–21] However, these commonly used methods cannot accurately quantify the size or purity of NFA-based BHJ domains due to the low contrast of the constituent compositionally similar materials.^[22,23] Resonant soft X-ray scattering (R-SoXS) studies of NFA BHJs have reported scattering peaks at $q < 0.1 \text{ nm}^{-1}$, indicating large donor- or acceptor-rich areas are present and suggesting a characteristic mode length in the acceptor phase as large as 90 nm.^[23] Although R-SoXS is a widely used and powerful tool, many of the organic semiconductor–X-ray interactions result in high-energy electrons that cause damage to the native structure.^[24] As such, a convenient, benign probe to quantify the size of donor and acceptor domains in BHJs is in high demand not only for understanding the effect of domain size on device relevant figures of merit such as PCE, but also to provide researchers with the ability to probe morphological changes to BHJs under various conditions in the absence of probe-induced degradation.

In this work, we present a novel photoluminescence-based quasi-steady-state measurement technique to quantify the domain size and exciton dissociation efficiency in BHJs. This technique is validated through Monte-Carlo simulations and experiments, and further used to quantify the acceptor domain size in technologically relevant BHJs. We find that NFA-based BHJs form larger acceptor domains than fullerene-based systems. However, these domains are not large enough to explain

the observed non-Langevin recombination rates based upon geometrical confinement of charges. Instead, the ratio of exciton diffusion length to average domain size is found to be a figure of merit that correlates well with reduced bimolecular recombination. This indicates that efficient exciton dynamics enable strongly reduced bimolecular recombination in high-efficiency NFA-based organic solar cells with low energetic offsets.

2. Analytical Construct

The charge generation process for an exciton in the donor phase of an FRET-activated BHJ is shown in **Figure 1a**. The photoexcited exciton diffuses freely throughout the donor phase until it is within the FRET radius (R_{FRET}) of the donor–acceptor interface, at which point the exciton is transferred to the acceptor phase with a high probability of arriving near the interface. Hence, from the exciton’s frame of reference, the donor domain size is smaller than the phase separation of the BHJ by twice R_{FRET} . Since FRET from the NFA to the donor is typically inefficient in most state-of-the-art BHJs, excitons generated in the acceptor phase (or transferred there via FRET) diffuse within the acceptor phase before reaching the interface and dissociating into a CT state. Conversely, **Figure 1b** shows a corresponding schematic of the bimolecular recombination process occurring in the same system. Since the electron and hole are free to diffuse everywhere in their respective domains, the donor domain size in the charge-carrier frame of reference is equivalent to the phase-separated domain size and thus larger than the donor domain in the frame of reference of an exciton. In the ideal BHJ, defined by a fully percolated donor–acceptor network with well-defined interfaces, the characteristic mode length, as defined in R-SoXS experiments, and domain size, as defined by L in **Figure 1b**, are equivalent. Total scattering intensity approaching unity from R-SoXS experiments indicates a high domain purity in the fullerene and NFA-based systems studied here, signifying that these systems are closely approximated by this ideal form.^[23,25–27]

To probe the domain size, a photoluminescence-based method has been developed, based on measuring the density dependence of the relative photoluminescence quantum yield (PLQY, η_{PL}) of excitons under quasi-steady-state excitation conditions. At high excitation densities, excitons interact via exciton–exciton annihilation (EEA) providing a nonlinear, nonradiative relaxation

channel, reducing η_{PL} .^[28] The rate equation for the density of excitons (ρ) in one phase of a BHJ is given by

$$\frac{d\rho}{dt} = -\frac{\rho}{\tau} - k_{\text{eff}}\rho - \gamma\rho^2 \quad (1)$$

where τ is the exciton lifetime in the neat semiconductor of the corresponding phase, k_{eff} is the effective rate of energy or charge transfer from the occupied phase to the opposing phase, and $\gamma = 4\pi DR_0$ is the EEA rate constant, in which D and R_0 are the diffusion constant and exciton capture radius (taken as the d_{100} spacing given by grazing-incidence X-ray diffraction measurements) of the occupied phase, respectively.^[28–30] In the case of a phase-separated BHJ, the effective rate of charge or energy transfer is dependent on the efficiency of exciton diffusion toward the donor–acceptor interface ($\eta_{\text{diff}} = (2L_D/L) \tanh(L/2L_D)$, in which $L_D = \sqrt{D\tau}$ is the exciton diffusion length) and the rate of exciton extraction at the (effective) interface.^[17] The exciton extraction occurs either as a charge transfer at the interface, historically assumed to depend on the energetic offset between the exciton and CT state, or as an energy transfer near the interface, dictated by the FRET rate.

The photoluminescence quantum efficiency, corresponding to the ratio between the total number of excitons decaying radiatively and the total number of generated excitons, is given by $\eta_{\text{PL}} = [\eta_{\text{PL},0} \int_0^\infty \rho(t) dt / \tau_{\text{eff}}] / \rho_0$ where $\eta_{\text{PL},0}$ is the photoluminescence quantum efficiency at low excitation densities, ρ_0 the initial density of excitons, and $\tau_{\text{eff}} = \tau / (1 + \tau k_{\text{eff}})$.^[17,28] In each individual phase, the density-dependent η_{PL} is then obtained by solving Equation (1) and integrating to yield

$$\eta_{\text{PL}} = \eta_{\text{PL},0} \frac{\ln[1 + \rho_0 \gamma \tau_{\text{eff}}]}{\rho_0 \gamma \tau_{\text{eff}}} \quad (2)$$

By measuring the relative change ($\eta_{\text{PL}}/\eta_{\text{PL},0}$) in PLQY as a function of ρ_0 generated via an instantaneous source, referred to as pulsed-PLQY, $\gamma\tau_{\text{eff}}$ can be extracted through Equation (2). In the case of a neat organic semiconductor ($k_{\text{eff}} = 0$, $\tau_{\text{eff}} = \tau$), pulsed-PLQY can be used to measure the exciton diffusion length as $L_D = \sqrt{\gamma\tau/4\pi R_0}$.^[28] In a BHJ film, the efficiency of exciton quenching can be expressed as the competition between the effective extraction rate and the natural decay rate $P_S = k_{\text{eff}}(k_{\text{eff}} + 1/\tau)$. Under conditions where the rate of charge or FRET transfer is efficient, the system becomes diffusion-limited, and $\gamma\tau_{\text{eff}}$ in the occupied phase can be related to the domain size through^[17]

$$P_S = 1 - \frac{\gamma\tau_{\text{eff}}}{\gamma\tau} = \frac{2L_D}{L} \tanh\left[\frac{L}{2L_D}\right] \quad (3)$$

Consequently, by measuring $\gamma\tau$ in a neat semiconductor and $\gamma\tau_{\text{eff}}$ from the corresponding phase of a BHJ using pulsed-PLQY, Equation (3) can be solved, and the average domain size L can be calculated, analogous to the characteristic mode length measured in an R-SoXS experiments. Although distinct quenching experiments have been used historically to evaluate P_S , these techniques often suffer from complications related to evaluating the excitation density and the resulting density dependence of the exciton kinetics. Utilizing pulsed-PLQY, P_S can be evaluated with a high degree of confidence in a density-independent manner.

3. Results

3.1. Validation of Domain Size Probe

The efficacy of the technique laid out above was validated in three ways: 1) by applying the method to simulated results with known domain size and diffusion length through Monte-Carlo simulations; 2) by applying the method to bilayer systems for which the domain size, reflected by the thickness of each layer, can be measured independently by other means; and 3) by applying the method to a benchmark BHJ system for which the domain size is previously estimated using other techniques.

Monte-Carlo simulations were chosen as they have been shown to accurately account for exciton dynamics within organic semiconductors and BHJs.^[28,31,32] The Monte-Carlo simulations were conducted in an infinite cylinder geometry to simulate a single domain in a percolated BHJ, with the domain size being defined as the diameter of the cylinder. Although many BHJs show inhomogeneous regions of donor–acceptor mixing, the choice of a sharp boundary was used to validate the experimental procedure under ideal conditions, where the domain size is known precisely. Simulated exciton dynamics within the domain included natural decay and annihilation, while excitons at the domain edge were additionally subject to extraction and reinjection. The PLQY of the simulation was defined as the ratio of excitons decaying radiatively to the total number of excitons generated in the simulation. For further details on the Monte-Carlo simulations, see Section S4.1 (Supporting Information).

Figure 2a shows the results of the Monte-Carlo simulations where the black dashed line indicates Equation (2) for a neat film, and the circles (dashed lines) indicate the simulated $\eta_{\text{PL}}/\eta_{\text{PL},0}$ (fits to Equation (2)) for simulations with varying domain diameter. When the domain diameter is large, compared to L_D , there is little charge or energy transfer occurring (green curve, Figure 2a). This corresponds to the case of a small P_S and k_{eff} , while $\tau_{\text{eff}} \approx \tau$; hence, there is little change in $\eta_{\text{PL}}/\eta_{\text{PL},0}$ from the case of a neat film. On the other hand, when the domain diameter is small (blue curve, Figure 2a), charge or energy transfer from the domain increases, resulting in an increase of both P_S and k_{eff} . Consequently, τ_{eff} decreases causing the onset of the reduction in $\eta_{\text{PL}}/\eta_{\text{PL},0}$ to shift to higher densities. Fitting each simulated curve to Equation (2) and solving Equation (3) for L agrees well with the input diameter across the considered range of diameters. This agreement is depicted in the inset of Figure 2a, where the fitted domain size coincides well with the input domain diameter across a wide range.

Next, to experimentally validate Equations (2) and (3), a series of bilayer films (mimicking the domain size in BHJs) were fabricated with a glass/acceptor/donor structure with 2,2'-[[12,13-Bis(2-butyloctyl)-12,13-dihydro-3,9-dinonylbisthieno[2'',3'':4',5']-thieno[2',3':4,5]pyrrolo[3,2-e:2',3'-g][2,1,3]benzothiadiazole-2,10-diyl]bis[methylidyne(5,6-chloro-3-oxo-1-H-idene-2,1(3H)-diylidene)]bis[propanedinitrile] (Y6) as the acceptor and poly[4,8-bis(5-(2-ethylhexyl)thiophen-2-yl)benzo[1,2-b;4,-5b']dithiophene-2,-6-diyl-alt-(4-(2-ethylhexyl)-3-fluorothieno[3,4-b]thiophene)-2-carboxylate-2,6-diyl](PTB7-Th) as the donor using the spontaneous spreading method (see Section S1 for a list of chemical definitions and Section S2.2 for details).^[33,34] The resulting Y6 layers had a well-defined and controllable thickness and a sharp

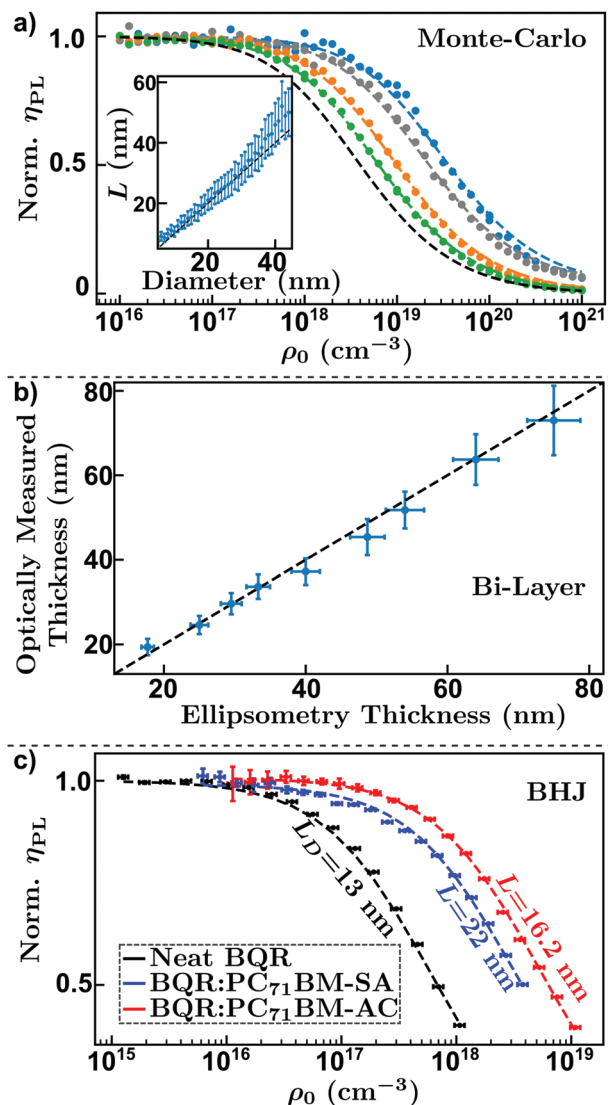


Figure 2. Validation of the photoluminescence-based domain size measurement technique. a) Monte-Carlo simulated pulsed-PLQY data for varying domain sizes (colored circles) and Equation (2) plotted for a neat film (black dashed line) and fit to simulated data (colored lines). Inset: simulated measured domain diameter as a function of input domain diameter. b) Film thickness measured via pulsed-PLQY as a function of ellipsometry measured film thickness for a series of Y6/PTB7-Th bilayers taken from pulsed-PLQY data (Figure S4, Supporting Information). c) Pulsed-PLQY data (circles) and fit to Equation (2) (dashed lines) for neat BQR (black) and BQR:PC₇₁BM bulk-heterojunction thin films, as cast (AC, red) and solvent annealed (SA, blue). Indicated are the measured diffusion length and domain sizes.

interface with the PTB7-Th layer. These materials were selected to ensure that there is efficient charge transfer at the interface and that, under quasi-steady-state conditions, the majority of excitons were generated within the Y6 phase. Pulsed-PLQY was conducted on a neat Y6 film and a series of bilayer films with Y6 thickness varying from 17 to 75 nm, and the resulting $\gamma\tau_{\text{eff}}$ was used to calculate the thickness of the Y6 layer (akin to the domain size in BHJs) using pulsed-PLQY through a modified Equation (3) (Figure S4, Supporting Information). Figure 2b

shows the results of these experiments. The thicknesses obtained from pulsed-PLQY are in excellent agreement with the thickness measured via ellipsometry.

Finally, to further substantiate pulsed-PLQY as a tool to quantify the domain size in BHJs, we applied the method to a model BHJ system for which the domain size is known from other techniques. For this purpose, we chose benzodithiophene-*quaterthiophene*-rhodanine (BQR) as a donor and [6,6]-phenyl-C₇₁-butyric acid methyl ester (PC₇₁BM) to make BQR:PC₇₁BM for which the domain size has previously been found to be 15 nm in as cast (AC) blends.^[35] We examined AC films as well as those prepared with solvent annealing (SA). To ensure the quality of our BQR devices we fabricated BQR:PC₇₁BM solar cells with PCEs of 4.79% and 9.33%, respectively, for AC and SA devices (Figure S5, Supporting Information); these PCEs are close to previous reports.^[35,36] We then applied pulsed-PLQY on the BHJs as well as neat BQR films. Figure 2c shows the results of these experiments. The black curve shows the normalized $\eta_{\text{PL}}/\eta_{\text{PL},0}$ obtained from the neat SA-BQR film. Both SA and AC neat BQR films were found to have equivalent L_{D} , consistent with previous findings.^[35] In the case of the BHJ blends, we obtained a domain size of 16.2 ± 0.7 nm for the AC BHJ, which is very close to the previous report of 15 nm.^[35] Upon solvent annealing, the onset of the reduction in $\eta_{\text{PL}}/\eta_{\text{PL},0}$ shifts to lower densities indicating an enhancement in the domain size of the BQR phase to 22 ± 1 nm in the SA blend, again consistent with previous reports. However, we note that the exact domain size is strongly dependent on the SA conditions.

In conclusion, we validated our methodology for quantifying the domain size from pulsed-PLQY. The fitted domain size obtained from our method agrees well with the input parameters in the Monte-Carlo BHJ simulations. Also, thicknesses obtained from our method in bilayer experiments agree very well with thicknesses obtained from ellipsometry. Finally, applying our method to BQR:PC₇₁BM BHJs we obtained domain sizes in agreement with previous reports.

3.2. Domain Size of BHJs

Having validated pulsed-PLQY through three different methods, we utilize it to measure the domain size (L) in several technologically relevant systems compared to a fullerene-acceptor-based system. To measure pulsed-PLQY in one phase of a BHJ, the photoluminescence of this phase must be spectrally isolated. In the case of a heavily quenched fullerene system, such as a blend of poly[*N*-9'-heptadecanyl-2,7-carbazole-*alt*-5,5-(4'7'-di-2-thienyl-2',1',3'-benzothiadiazole)] (PCDTBT) as a donor and [6,6]-phenyl-C₆₁-butyric acid methyl ester (PC₆₁BM) as an acceptor to make PCDTBT:PC₆₁BM, the emission of the BHJ is due only to emission from the PC₆₁BM phase (photoluminescence spectra are shown in Figures S6 and S7 in the Supporting Information). Figure 3a shows pulsed-PLQY data taken on a neat PC₆₁BM (black circles) and a PCDTBT:PC₆₁BM BHJ (red circles) film; the black and red dashed lines indicate fittings to Equation (2). The shift in the onset of the reduction in $\eta_{\text{PL}}/\eta_{\text{PL},0}$ is indicative of phase separation in the BHJ. Solving Equation (3) indicates that $L = 9.0 \pm 0.6$ nm for the PC₆₁BM phase of PCDTBT:PC₆₁BM.

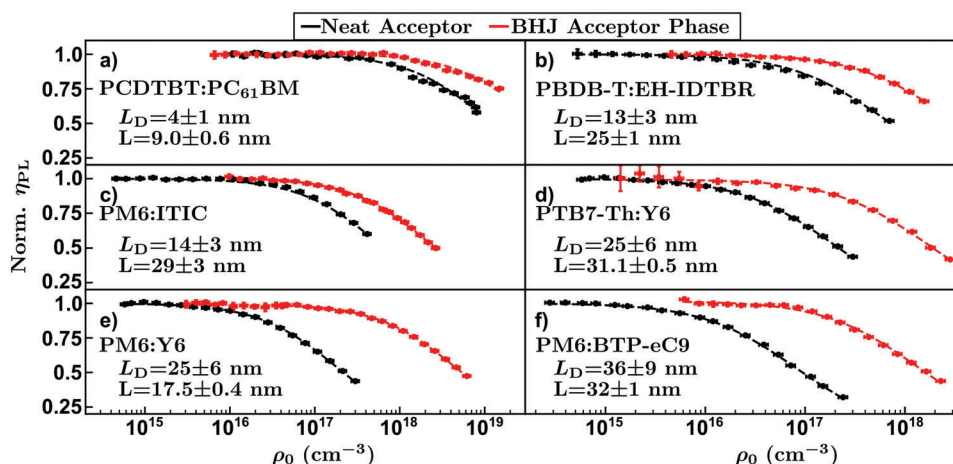


Figure 3. Pulsed-PLQY data. a–f) Relative photoluminescence quantum yield as a function of initial excitation density measured on (black circles) neat acceptor films and (red circles) acceptor phase of BHJ films. Black and red lines indicate fittings to Equation (3). Inset shows the extracted exciton diffusion length for neat acceptor films and acceptor domain size for BHJ films.

A series of low-offset NFA-based systems were fabricated using PTB7-Th, poly[(2,6-(4,8-bis(5-(2-ethylhexyl-3-fluoro)thiophen-2-yl)-benzo[1,2-b:4,5-b']dithiophene))-*alt*-(5,5-(1',3'-di-2-thienyl-5',7'-bis(2-ethylhexyl)benzo[1',2'-c:4',5'-c']dithiophene-4,8-dione)) (PM6), and poly[[4,8-bis(5-(2-ethylhexyl)-2-thienyl)benzo[1,2-b:4,5-b']dithiophene-2,6-diyl]-2,5-thiophene diyl[5,7-bis(2-ethylhexyl)-4,8-dioxo-4H,8H-benzo[1,2-c:4,5-c']dithiophene-1,3-diyl]] (PBDBT) as donors and Y6, 3,9-bis(2-methylene-(3-(1,1-dicyanomethylene)-indanone))5,5,11,11-tetrakis(4-hexylphenyl)-dithieno[2,3-d:2',3'-d']-s-indaceno[1,2-b':5,6-b']dithiophene (ITIC), (5Z)-3-ethyl-2-sulfanylidene-5-[[4-[9,9,18,18-tetrakis(2-ethylhexyl)-15-7-[(Z)-(3-ethyl-4-oxo-2-sulfanylidene-1,3-thiazolidin-5-ylidene)methyl]-2,1,3-benzothiadiazole-4-yl]-5,14-dithiapentacyclo[10.6.0.0.3,10.0.4,8.0.13,17]octadeca-1(12),2,4(8),6,10,13(17),15-heptaen-6-yl]-2,1,3-benzothiadiazol-7-yl]methylidene]-1,3-thiazolidin-4-one (EH-IDTBR) and 2,2'-[[12,13-bis(2-butyloctyl)-12,13-dihydro-3,9-dinoonylbisthieno[2'',3'':4'5']thieno[2',3':4,5]pyrrolo[3,2-e:2',3'-g][2,1,3]benzothiadiazole-2,10-diyl]bis[methylidyne(5,6-chloro-3-oxo-1H-indene-2,1(3H)-diylidene)]]bis[propanedinitrile] (BTP-eC9) as acceptors to make PTB7-Th:Y6, PM6:ITIC, PBDBT:EH-IDTBR, PM6:Y6, and PM6:BTP-eC9. In all these systems the quasi-steady-state photoluminescence spectra included emission from both the donor and acceptor phases. Therefore, by using appropriate low- and high-pass filters in the collection pathway it is possible to collect emission from the donor and acceptor phases, respectively, and in principle measure the domain size of both phases independently. However, the relative heights of the emission from the donor and acceptor phases indicate that the absorbed light does not create an equal population of excitons in each phase. The density of excitons available for EEA in each phase can be calculated from the quasi-steady-state absorption via the relative heights of the photoluminescence spectra and the absolute value of $\eta_{PL,0}$ of each neat semiconductor (see Section S6.1 in the Supporting Information for details). For each of the donor:NFA systems studied, this analysis indicated that >95% of all excitons are available for EEA in the acceptor phase.

Once the appropriate high-pass filter was chosen for each system, pulsed-PLQY was performed on neat acceptor films and high-pass-filtered NFA-based BHJs, accounting for the uneven population of excitons. Figure 3b–f shows pulsed-PLQY data taken on long-pass-filtered NFA-based BHJs and the associated neat acceptor. The resulting fits to $\gamma\tau$ and $\gamma\tau_{\text{eff}}$ were used, in conjunction with Equation (3), to solve for the size of the acceptor domain. The label in each panel of Figure 3 indicates the measured L_D of the neat acceptor, and the extracted average domain size in the acceptor phase. Total scattering intensities approaching unity for each of these systems indicate pure domains that are closely approximated by Figure 1a signifying that the extracted average domain size is emblematic of the average domain spacing.^[23,25–27] Notably, pure domains much larger than PC₆₁BM were measured in all NFA systems studied, indicating that NFA-based BHJs naturally form large (>17 nm) domains.

Due to the high absorption in the acceptor phase, pulsed-PLQY in the donor phase resulted in photo-oxidation of films at densities below the onset of the reduction of η_{PL} , indicating that this analysis was not possible in the heavily quenched donor phase (see Section S7 in the Supporting Information for details). Therefore, L in the donor phase can, in this case, only be estimated indirectly by considering the ratio of the height of the donor photoluminescence signal in the BHJ (Φ_{BHJ}) to the neat film (Φ_{neat}). Further, efficient FRET from the donor to the acceptor phase has been observed in many low-offset NFA-based systems;^[9] therefore, the domain size of the donor estimated from the photoluminescence quenching is indicative of L_{eff} , seen from the frame of reference of excitons. The domain size defined in Figure 1b can be estimated as $L = L_{\text{eff}} + 2R_{\text{FRET}}$. The donor-to-acceptor R_{FRET} was measured in PTB7-Th:Y6, PM6:Y6, and PM6:BTP-eC9, and found to be 3.9, 3.7, and 2.9 nm, respectively (see Section S8 in the Supporting Information for details). Taking this into account, the phase-separated donor domains were estimated to be ≈ 10 nm in all systems studied.

4. Discussion

The above results show that NFA domain sizes are substantially larger than the 9.0 ± 0.6 nm measured in the fullerene system PCDTBT:PC₆₁BM and, evidently, larger than the expected Coulomb capture radii for organic semiconductors.^[37] This observation precipitates questions about the relevance of charge encounter dynamics to the device performance in state-of-the-art NFA–BHJ OPVs. A semiempirical formula can be used to estimate ζ_{enc} if both charge-carrier mobilities and domain size are known (see Section S10 in the Supporting Information).^[14] Based on the measured acceptor domain size and mobilities (see Section S9 in the Supporting Information), we obtained that $\zeta_{\text{enc}} < 3$ for all systems (Table S3, Supporting Information), indicating that charge encounter dynamics have little influence over the total bimolecular recombination reduction factors.

An elucidating comparison can be drawn between the highest PCE systems, PM6:Y6 (Figure 3e) and PM6:BTP-eC9 (Figure 3f). The exciton diffusion length in neat Y6 was found to be 25 ± 6 nm, while the exciton quenching efficiency in the PM6:Y6 BHJ was found to be 0.960 ± 0.005 , leading to an extracted domain size of 17.5 ± 0.4 nm. Similar domain sizes have been inferred from R-SoXS experiments.^[38] Comparing this to PM6:BTP-eC9, BTP-eC9 has a larger diffusion length ($L_D = 36 \pm 9$ nm) while the PM6:BTP-eC9 BHJ shows a similar exciton dissociation efficiency (0.94 ± 0.01), resulting in a domain size of 32 ± 1 nm, almost twice that of PM6:Y6. We note that R_{FRET} for acceptor-to-donor energy transfer was found to be below the intermolecular spacing of the acceptor for these materials, indicating that the L measured in the frame of reference of excitons localized to the acceptor phase is representative of the corresponding phase separation (see Section S9, Supporting Information).

For PM6:Y6 and PM6:BTP-eC9, $\zeta_{\text{enc}} \approx 2$ was obtained for both systems. This contrasts with measured values for ζ_1 of 400 and 1000 for PM6:Y6 and PM6:BTP-eC9, respectively, with ζ_1 being 2.5 times larger in PM6:BTP-eC9 than in PM6:Y6.^[10] According to the semiempirical formula, to increase the ζ_{enc} of PM6:Y6 by a factor of 2.5, the domain size would need to be ≈ 70 nm. In addition, to maintain $P_S > 0.96$ for a domain size of ≈ 70 nm would require an exciton diffusion length of $L_D \approx 100$ nm. Despite the recent surge in acceptor molecules with large L_D , materials matching these requirements are yet to be realized. Therefore, as previously suggested by others, the domain sizes are not large enough to explain the heavily reduced recombination in the highest-performing systems.^[12,14]

As discussed in various independent experimental reports, acceptors that form the highest efficiency systems (in this case Y6 and BTP-eC9) generally show longer exciton diffusion lengths compared to fullerene systems.^[28,30] However, this does not guarantee a high-performing system, as the other NFA-based systems studied here also show increased acceptor L_D (compared to fullerene systems), while only displaying modest PCEs. With this in mind, and in accordance with Equation (3), the relevant figure of merit for exciton diffusion in BHJs is instead the ratio of the diffusion length to the average domain size (L_D/L), sometimes referred to as the characteristic length ratio.^[17] In the case of PM6:BTP-eC9, the large acceptor domain size is not an impediment to charge generation due to the large diffusion length of BTP-eC9, while in the case of PM6:Y6 the smaller domain size

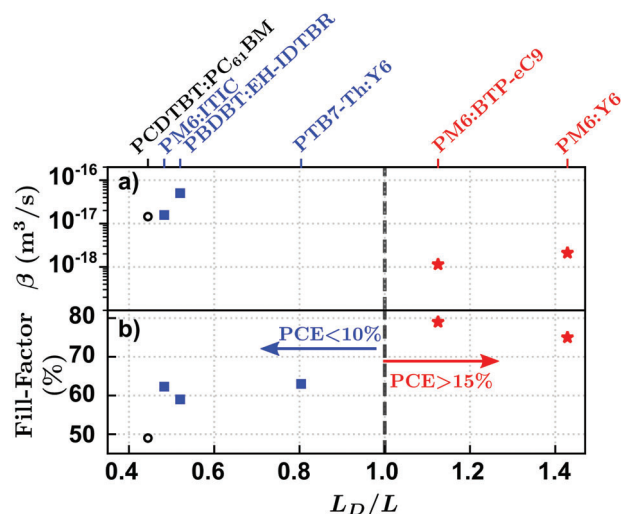


Figure 4. Characteristic length ratio dependency of recombination and fill factor. a) Bimolecular recombination constant, and b) fill factor measured for each system as a function of characteristic length ratio measured from pulsed-PLQY. Black open circles indicate fullerene-based systems; blue squares indicate NFA-based systems with PCE < 10%; and red stars indicate NFA-based systems with PCE > 15%. β for PCDTBT:PC₆₁BM was taken from ref. [40], no reliable measure of β was available for PTB7-Th:Y6 devices, all other β values were taken from ref. [10].

allows for high P_S with a reduced L_D . In the remaining systems, acceptor domain sizes greater than that measured in PM6:Y6, coupled with decreased diffusion lengths (<16 nm), contributed to lower short-circuit currents and fill factors (FF) (corresponding current–voltage characteristics are provided in Figure S5 in the Supporting Information).

To explore the relevance of the characteristic length ratio to device performance, **Figure 4a** shows the total bimolecular recombination rate constant, and **Figure 4b** shows the FF of each system studied as a function of L_D/L . For the systems with $L_D/L > 1$, β is reduced by an order of magnitude compared to those of $L_D/L < 1$, leading to improvements in FF, reflected in **Figure 4b**, and ultimately PCE. Importantly, NFA-based systems with large domain sizes or long exciton diffusion lengths do not necessarily exhibit strongly reduced bimolecular recombination; rather, the observed trend suggests that efficient exciton dynamics enable strongly reduced bimolecular recombination through enhanced ζ_{CT} . Delineating the mechanism of ζ_{CT} enhancement is beyond the scope of this work and is typically attributed to the interplay between the kinetic rate constants of exciton re-dissociation and decay, including triplet CT states and triplet excitons.^[15,39] This observation indicates that the processes that facilitate effective exciton dissociation are the same processes that reduce bimolecular recombination in efficient NFA-based solar cells. Further, these processes are strongly dependent on both morphology and exciton dynamics while being only weakly dependent on the free-charge-carrier encounter dynamics. In other words, our findings imply that exciton dynamics play a decisive role in non-Langevin charge-carrier recombination in NFA solar cells based on low-offset systems. This highlights the importance of not only pure domains for efficient charge-carrier generation and extraction, but also of a thorough understanding of the exciton dynamics occurring within donor and acceptor domains.

5. Conclusion

Pulsed-PLQY was shown to be a viable, accurate, and benign probe to quantify the acceptor domain size in both fullerene- and NFA-based BHJs. Based on this technique, NFAs were found to exhibit longer exciton diffusion lengths and form larger domains, when blended with an appropriate donor, than their fullerene counterparts. However, these characteristics alone are not enough to form a high-efficiency BHJ OPV-based solar cell. Instead, the ratio of exciton diffusion length to average domain size correlates to increased suppression of the bimolecular recombination rate constant leading to improved FFs. Notably, the highest-performing systems (PM6:Y6 and PM6:BTP-eC9) were both found to have a ratio greater than 1, indicating that this is an important design rule for phase-separated OPV-based solar cells. Further, these results suggest that the processes engendering strongly reduced bimolecular recombination are enabled by and related to efficient exciton dynamics.

Supporting Information

Supporting Information is available from the Wiley Online Library or from the author.

Acknowledgements

This work was supported by the Welsh Government's Sêr Cymru II Program through the European Regional Development Fund, Welsh European Funding Office, and the Swansea University strategic initiative in Sustainable Advanced Materials. A.A. is a Sêr Cymru II Rising Star Fellow, and P.M. is a Sêr Cymru II National Research Chair. This work was also funded by UKRI through the EPSRC Program Grant EP/T028513/1 Application Targeted Integrated Photovoltaics. D.B.R. acknowledges the support of the Natural Sciences and Engineering Research Council of Canada (NSERC) (Grant No. PGSD3-545694-2020)).

Conflict of Interest

The authors declare no conflict of interest.

Data Availability Statement

The data that support the findings of this study are available from the corresponding author upon reasonable request.

Keywords

bimolecular recombination, domain size, exciton diffusion, organic solar cells, organic photovoltaics

Received: November 30, 2022

Revised: March 5, 2023

Published online: May 1, 2023

- [1] Y. Cai, Y. Li, R. Wang, H. Wu, Z. Chen, J. Zhang, Z. Ma, X. Hao, Y. Zhao, C. Zhang, F. Huang, Y. Sun, *Adv. Mater.* **2021**, *33*, 2101733.
 [2] Q. Liu, Y. Jiang, K. Jin, J. Qin, J. Xu, W. Li, J. Xiong, J. Liu, Z. Xiao, K. Sun, S. Yang, X. Zhang, L. Ding, *Sci. Bull.* **2020**, *65*, 272.
 [3] Y. Cui, Y. Xu, H. Yao, P. Bi, L. Hong, J. Zhang, Y. Zu, T. Zhang, J. Qin, J. Ren, Z. Chen, C. He, X. Hao, Z. Wei, J. Hou, *Adv. Mater.* **2021**, *33*, 2102420.

- [4] A. Armin, W. Li, O. J. Sandberg, Z. Xiao, L. Ding, J. Nelson, D. Neher, K. Vandewal, S. Shoaee, T. Wang, H. Ade, T. Heumüller, C. Brabec, P. Meredith, *Adv. Energy Mater.* **2021**, *11*, 2003570.
 [5] O. J. Sandberg, A. Armin, *J. Phys. Chem. C* **2021**, *125*, 15590.
 [6] A. Armin, I. Kassal, P. E. Shaw, M. Hamsch, M. Stolterfoht, D. M. Lyons, J. Li, Z. Shi, P. L. Burn, P. Meredith, *J. Am. Chem. Soc.* **2014**, *136*, 11465.
 [7] T. M. Clarke, J. R. Durrant, *Chem. Rev.* **2010**, *110*, 6736.
 [8] T. Förster, *Ann. Phys.* **1948**, *437*, 55.
 [9] S. Karthedath, J. Gorenflot, Y. Firdaus, N. Chaturvedi, C. S. P. De Castro, G. T. Harrison, J. I. Khan, A. Markina, A. H. Balawi, T. A. D. Peña, W. Liu, R. Z. Liang, A. Sharma, S. H. K. Paleti, W. Zhang, Y. Lin, E. Alarousu, S. Lopatin, D. H. Anjum, P. M. Beaujuge, S. De Wolf, I. McCulloch, T. D. Anthopoulos, D. Baran, D. Andrienko, F. Laquai, *Nat. Mater.* **2021**, *20*, 378.
 [10] W. Li, S. Zeiske, O. J. Sandberg, D. B. Riley, P. Meredith, A. Armin, *Energy Environ. Sci.* **2021**, *14*, 6484.
 [11] L. Perdigon-Toro, H. Zhang, A. Markina, J. Yuan, S. M. Hosseini, C. M. Wolff, G. Zuo, M. Stolterfoht, Y. Zou, F. Gao, D. Andrienko, S. Shoaee, D. Neher, *Adv. Mater.* **2020**, *32*, 1906763.
 [12] A. Armin, J. Subbiah, M. Stolterfoht, S. Shoaee, Z. Xiao, S. Lu, D. J. Jones, P. Meredith, *Adv. Energy Mater.* **2016**, *6*, 1600939.
 [13] G. Juška, K. Arlauskas, J. Stuchlik, R. Österbacka, *J. Non-Cryst. Solids* **2006**, *352*, 1167.
 [14] M. C. Heiber, C. Baumbach, V. Dyakonov, C. Deibel, *Phys. Rev. Lett.* **2015**, *114*, 136602.
 [15] S. Shoaee, A. Armin, M. Stolterfoht, S. M. Hosseini, J. Kurpiers, D. Neher, *Sol. RRL* **2019**, *3*, 1900184.
 [16] A. Classen, C. L. Chochos, L. Luer, V. G. Gregoriou, J. Wortmann, A. Osvet, K. Forberich, I. McCulloch, T. Heumüller, C. J. Brabec, *Nat. Energy* **2020**, *5*, 711.
 [17] D. B. Riley, P. Meredith, A. Armin, O. J. Sandberg, *J. Phys. Chem. Lett.* **2022**, *13*, 4402.
 [18] A. Karki, J. Vollbrecht, A. J. Gillett, S. S. Xiao, Y. Yang, Z. Peng, N. Schopp, A. L. Dixon, S. Yoon, M. Schrock, H. Ade, G. N. M. Reddy, R. H. Friend, T.-Q. Nguyen, *Energy Environ. Sci.* **2020**, *13*, 3679.
 [19] O. K. Kwon, M. A. Uddin, J.-H. Park, S. K. Park, T. L. Nguyen, H. Y. Woo, S. Y. Park, *Adv. Mater.* **2016**, *28*, 910.
 [20] H. Yao, L. Ye, J. Hou, B. Jang, G. Han, Y. Cui, G. M. Su, C. Wang, B. Gao, R. Yu, H. Zhang, Y. Yi, H. Y. Woo, H. Ade, J. Hou, *Adv. Mater.* **2017**, *29*, 1700254.
 [21] X. Yi, Z. Peng, B. Xu, D. Seyitliyev, C. H. Y. Ho, E. O. Danilov, T. Kim, J. R. Reynolds, A. Amassian, K. Gundogdu, H. Ade, F. So, *Adv. Energy Mater.* **2020**, *10*, 1902430.
 [22] F. Zhao, C. Wang, X. Zhan, *Adv. Energy Mater.* **2018**, *8*, 1703147.
 [23] L. Ye, W. Zhao, S. Li, S. Mukherjee, J. H. Carpenter, O. Awartani, X. Jiao, J. Hou, H. Ade, *Adv. Energy Mater.* **2017**, *7*, 1602000.
 [24] J. H. Carpenter, A. Hunt, H. Ade, *J. Electron Spectrosc. Relat. Phenom.* **2015**, *200*, 2.
 [25] A. C. Stuart, J. R. Tumbleston, H. Zhou, W. Li, S. Liu, H. Ade, W. You, *J. Am. Chem. Soc.* **2013**, *135*, 1806.
 [26] K. Jiang, Q. Wei, J. Y. L. Lai, Z. Peng, H. K. Kim, J. Yuan, L. Ye, H. Ade, Y. Zou, H. Yan, *Joule* **2019**, *3*, 3020.
 [27] J.-W. Lee, C. Lim, S.-W. Lee, Y. Jeon, S. Lee, T.-S. Kim, J.-Y. Lee, B. J. Kim, *Adv. Energy Mater.* **2020**, *12*, 2202224.
 [28] D. B. Riley, O. J. Sandberg, W. Li, P. Meredith, A. Armin, *Phys. Rev. Appl.* **2022**, *17*, 024076.
 [29] S. Chandrasekhar, *Rev. Mod. Phys.* **1943**, *15*, 1.
 [30] M. T. Sajjad, A. Ruseckas, L. K. Jagadamma, Y. Zhang, I. D. W. Samuel, *J. Mater. Chem. A* **2020**, *8*, 15687.
 [31] H. Bässler, *Phys. Status Solidi B* **1993**, *175*, 15.
 [32] W. Kaiser, J. Popp, M. Rinderle, T. Albes, A. Gagliardi, *Algorithms* **2018**, *11*, 37.

- [33] F. J. M. Colberts, M. M. Wienk, R. Heuvel, W. Li, V. M. Le Corre, L. J. A. Koster, R. A. J. Janssen, *Adv. Energy Mater.* **2018**, *8*, 1802197.
- [34] T. H. Lee, W.-W. Park, S. Y. Park, S. Cho, O.-H. Kwon, J. Y. Kim, *Sol. RRL* **2021**, *5*, 2100326.
- [35] M. T. Sajjad, Y. Zhang, P. B. Geraghty, V. D. Mitchell, A. Ruseckas, O. Blaszczyk, D. J. Jones, I. D. W. Samuel, *J. Mater. Chem. C* **2019**, *7*, 7922.
- [36] N. Zarrabi, O. J. Sandberg, C. Kaiser, J. Subbiah, D. J. Jones, P. Meredith, A. Armin, *J. Phys. Chem. Lett.* **2020**, *11*, 10519.
- [37] L. Duan, Y. Zhang, H. Yi, F. Haque, R. Deng, H. Guan, Y. Zou, A. Uddin, *Energy Technol.* **2020**, *8*, 1900924.
- [38] Q. Liu, J. Fang, J. Wu, L. Zhu, X. Guo, F. Liu, M. Zhang, *Chin. J. Chem.* **2021**, *39*, 1941.
- [39] A. Privitera, J. Grüne, A. Karki, W. K. Myers, V. Dyakonov, T. Q. Nguyen, M. K. Riede, R. H. Friend, A. Sperlich, A. J. Gillett, *Adv. Energy Mater.* **2022**, *12*, 2103944.
- [40] M. Stolterfoht, A. Armin, S. Shoaee, I. Kassal, P. Burn, P. Meredith, *Nat. Commun.* **2016**, *7*, 11944.